

Operational Reliability of Integrated Energy Systems Considering Gas Flow Dynamics and Demand-Side Flexibilities

Sheng Wang , Member, IEEE, Junyi Zhai , Member, IEEE, Hongxun Hui , Member, IEEE, Yi Ding , Member, IEEE, and Yonghua Song , Fellow, IEEE

Abstract—The interdependency among the electricity, gas, heat, and cooling energy systems is ever-increasing. The flexible energy utilization patterns on the demand side and gas flow dynamics in the transmission system bring both opportunities and challenges to the reliable operation of integrated energy systems (IES). For example, if the electricity supply is interrupted, the gas system can ramp up the gas supply to the gas-fired units using linepacks. By this means, the reliability of the electricity system at this moment can be improved, while the gas system's capability of withstanding future risks may be undermined. Therefore, the operational reliability between different energy systems and time periods should be carefully balanced. This article proposes an operational reliability evaluation framework for the IES considering flexibilities from both the demand side and transmission system. First, the flexibilities of end-users and linepacks are explored based on the Energy Hub and gas flow dynamics models. Then, the reliability models of IES components are developed using the discretized-time Markov process to characterize the temporal state evolution in the operational horizon. A look-ahead contingency management scheme of the IES is then proposed to minimize the electricity and gas load curtailments. Taking account of all the possible system states, the operational reliabilities of the IES are evaluated using the time-sequential Monte Carlo simulation. Finally, the proposed method is validated by using the IEEE Reliability Test System and the practical Belgium gas transmission system.

Index Terms—Energy hub, flexibility, gas flow dynamics, integrated energy systems, operational reliability.

I. INTRODUCTION

COORDINATELY using multiple energies, e.g., electricity, gas, and heat, has been widely considered an effective solution to promote energy efficiency and decarbonize energy systems [1]. The concept of integrated energy systems (IES) is, thus, developed, as shown in Fig. 1 [2]. The IES comprises three layers: the supply side, transmission system, and demand side. The supply side includes gas-fired units, traditional fossil units, gas sources, and gas storages. The electricity and gas transmission systems, which are coupled by the gas-fired units, are also regarded as the integrated electricity and gas transmission systems (IEGTS). On the demand side, the end-users are located on electricity buses (EB) and gas buses (GB). They consume electricity and gas from IEGTS to satisfy their electricity, heat, and cooling demands [3]. This energy conversion process can be modeled using the concept of energy hub (EH) [4]. It provides a powerful tool to characterize the relationships between the multiple input and output energies in a unified form. The EH can have various configurations, including combined heat and power plant (CHP), gas boiler (GBL), and electric heat pumps (EHP), depending on the specific form of the energy system on the demand side.

However, the interdependency of multiple energies increases the complexity of maintaining the reliable operation of IES [5], which has become a research focus in recent years. The reliability studies for IES can be mainly divided into two categories: reliability of EH-based IES on the demand side [6], [7], [8], and reliability of IEGTS [9], [10], [11]. However, previous studies usually consider the impacts of supply-side facilities, while have not fully explored the impacts of gas flow dynamics in the transmission system and the demand-side flexibilities on the reliability of IES. In fact, these two factors are crucial for extending the feasible region of IES operation and improving operational reliability. The reasons are explained twofold as follows.

- 1) *In the transmission system*, the gas flow dynamics are much slower than the electric power flow [12]. When the upstream gas source fails and the gas supply is interrupted, the downstream end-users may still be able to consume

Manuscript received 24 March 2023; accepted 30 April 2023. Date of publication 12 May 2023; date of current version 19 January 2024. This work was supported in part by the Science and Technology Development Fund, Macau SAR under Grant SKL-IOTSC(UM)-2021-2023, Grant 0003/2020/AKP, and Grant 0117/2022/A3, and in part by the Natural Science Foundation of Jiangsu Province, China (Operational reliability evaluation of multisource and heterogeneous urban multienergy systems under Grant BK20220261). Paper no. TII-23-0992. (Corresponding authors: Hongxun Hui; Yi Ding.)

Sheng Wang, Hongxun Hui, and Yonghua Song are with the State Key Laboratory of Internet of Things for Smart City, Department of Electrical and Computer Engineering, University of Macau, Zhuhai 999078, China (e-mail: shengwang@um.edu.mo; hongxunhui@um.edu.mo; yhsong@um.edu.mo).

Junyi Zhai is with the College of New Energy, China University of Petroleum (East China), Qingdao 266580, China (e-mail: zhajunyi@upc.edu.cn).

Yi Ding is with the College of Electrical Engineering, Zhejiang University, Hangzhou 310027, China (e-mail: yiding@zju.edu.cn).

Color versions of one or more figures in this article are available at <https://doi.org/10.1109/TII.2023.3275712>.

Digital Object Identifier 10.1109/TII.2023.3275712

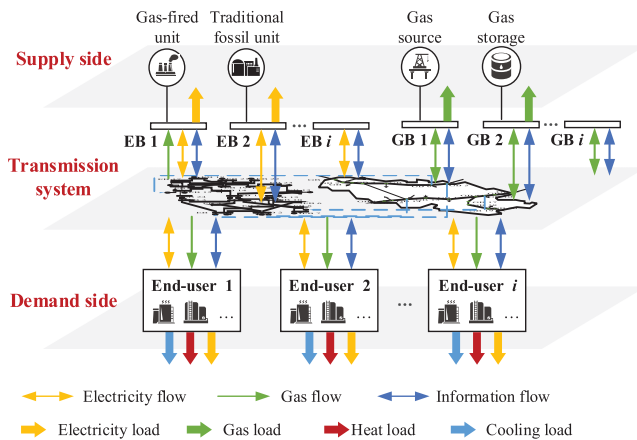


Fig. 1. Structure of the three-layer integrated energy system.

the gas stored in the pipeline (namely linepack) to satisfy the gas demand for a short period [13]. Therefore, the dynamics of the gas system can be regarded as a vital resource to accommodate gas demand spikes and enhance the reliability of IES. However, the overuse of linepack can also decrease the gas pressures of adjacent GBs, which may violate the minimum pressure requirement for gas transportation. Furthermore, the gas system will become more vulnerable to possible component failures in the following time periods if the linepack is abused and has not been complemented timely [14]. Therefore, it is challenging to manage the linepacks while improving and balancing the operational reliability of IES in different time periods.

- 2) *On the demand side*, end-users can choose among various electricity and gas consumption strategies to provide flexibility to the IES operation [15]. For example, the heat loads of end-users can be satisfied by the CHP and the EHP simultaneously. When the electricity supply is interrupted, CHP can ramp up its heat production and corresponding gas consumption, so that the EHP can reduce its heat production and corresponding electricity consumption [16]. This is also known as energy substitution [17]. By this means, the operational reliability of the electricity system can be improved. However, this energy substitution will increase gas consumption dramatically, which changes the gas flow pattern in the gas system and may jeopardize the operational reliability of the whole IES. Therefore, it is also challenging to use energy substitution properly for enhancing and balancing the reliability of the electricity and gas systems.

While the demand-side flexibilities and gas flow dynamics have been separately used to improve the operation [18], [19], unit commitment [20], [21], in the IES, only very few studies consider these two factors in the reliability evaluation. For example, on the demand side, the reliability model of the EH is first proposed in [22]. The impacts of initiative self-scheduling strategies of multienergy customers on operational reliability are studied in [23]. The multilinear parametric linear programming technique is applied to the EH to facilitate the reliability

evaluation efficiency in [24]. On the transmission side, the effect of lower dynamics of gas flow is demonstrated to be beneficial in improving the short-term reliability in [25]. The cascading effects of failure propagation between the electricity and gas systems with the gas flow dynamics, as well as their impacts on the reliability of the IES, are characterized in [26]. New reliability indices are proposed in [27] to quantify the impacts of time delays by the gas flow dynamics on the reliability of IES. However, the joint flexibilities of gas flow dynamics and demand side flexibilities have not been fully explored (e.g., using the linepack to cover the gas demand spikes generated by energy substitution). The opportunities in using these flexibilities to balance and improve the reliability of IES in terms of both different time periods and different energy systems have not been investigated either.

To address the research gap, this article contributes in the following aspects.

- 1) A novel operational reliability evaluation framework of the IES is proposed. Compared with traditional IES reliability evaluation studies, it can reveal the joint impacts of the gas flow dynamics and demand-side flexibilities on the temporal and spatial characteristics of the IES reliability.
- 2) A look-ahead contingency management scheme (LaCMS) is proposed, which can manage both the linepack and demand-side resources to minimize the load curtailments. By selecting different strategies and different linepack terminal conditions, it can realize the tradeoffs of IES reliability in terms of both different energy systems and different time periods.
- 3) A time-sequential Monte Carlo simulation procedure is designed for incorporating the chronological characteristics of both component state transitions and gas flow dynamics into the reliability evaluation. A forward-approximation-based linearization technique is developed and embedded in the inner loop of the Monte Carlo simulation to deal with the motion equation of gas flow dynamics in a tractable way.

II. OPERATIONAL RELIABILITY EVALUATION FRAMEWORK

The overall procedures of the operational reliability evaluation, and the mechanism of the reliability tradeoff are presented in Fig. 2. During the operation, the IES components (including the gas sources, gas storages, traditional fossil units, and gas-fired power plant) on the supply side may fail, causing the imbalance between the supply and demand in terms of both electricity and gas. The operational reliabilities of these IES components can be represented by multistate Markov models [28]. Compared with binary state models, which only involve perfect functioning state and complete failure state, the multistate model can provide a more flexible and accurate tool by considering degradation states. The feasible regions of EHs on the demand side, as well as the gas flow dynamics in the transmission system, are formulated to provide flexibilities to mitigate the imbalance between the supply and demand sides.

In the contingency states with component failures, the LaCMS is implemented. It follows two major ideas (as shown in Fig. 2)

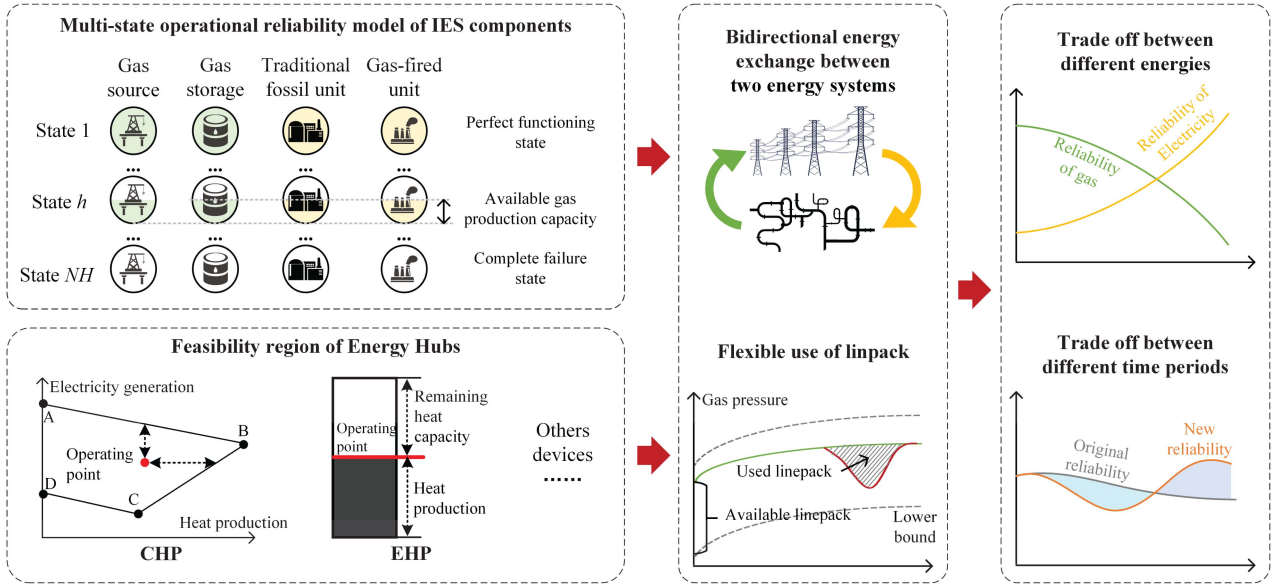


Fig. 2. Framework of operational reliability evaluation and the tradeoff effects in IES.

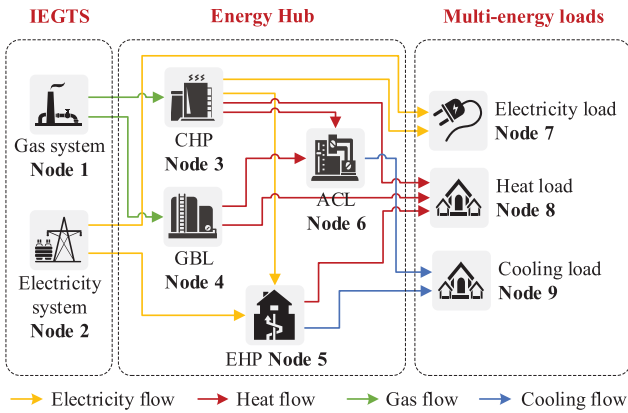


Fig. 3. Energy hub model of the end-user.

to promote the operational reliability of IES. First, by bidirectional energy exchange between the electricity and gas system via gas-fired generating units (and implicitly by changing the electricity and gas consumption profiles of EHs), one system can support another if it has redundancy. The second measure is to use linepack flexibly. By these two measures, the promotion and tradeoffs of reliabilities in terms of both different energy systems and time periods can be realized. Taking account of all possible scenarios by component failures, the operational reliability of IES can be evaluated.

III. MODELING OF IES FLEXIBILITIES

A. Flexibility of End-Users on the Demand Side

A typical EH model for end-users is shown in Fig. 3, which includes CHP, GBL, EHP, and absorption chiller (ACL). The electricity and gas transmission systems, devices in the EH, and multienergy loads are abstracted as nodes, respectively.

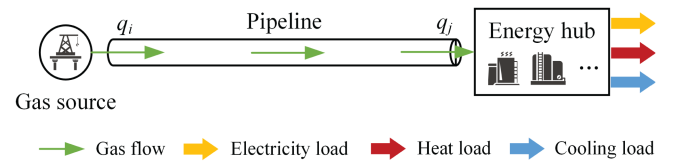


Fig. 4. Influence of gas flow dynamics on the feasible region of EH.

Based on the EH model, the feasible region can be defined as follows [8]:

$$\mathbf{H}\mathbf{x}^T = [\mathbf{0}_{1 \times 6}, d^{el} - lc^{el}, d^{hl} - lc^{hl}, d^{cl} - lc^{cl}]^T \quad (1)$$

$$\mathbf{A}\mathbf{x} + \mathbf{B} \leq \mathbf{0} \quad (2)$$

$$\mathbf{x} \geq \mathbf{0} \quad (3)$$

$$\mathbf{0} \leq [lc^{el}, lc^{hl}, lc^{cl}] \leq [lc^{el+}, lc^{hl+}, lc^{cl+}] \quad (4)$$

where \mathbf{H} is the energy conversion matrix; \mathbf{x} is the set of state variables; \mathbf{A} and \mathbf{B} are coefficient matrices. The specific forms of these matrices are illustrated in the Appendix. Superscript el , hl , and cl represent the energy types of electricity, heating, and cooling, respectively; d^{el} , d^{hl} , and d^{cl} are the electricity, heat, and cooling demands, respectively; lc^{el} , lc^{hl} , and lc^{cl} are the electricity, heat, and cooling curtailments, respectively; lc^{el+} , lc^{hl+} and lc^{cl+} represent the upper limits for electricity, heat, and cooling load curtailments, respectively.

B. Flexibility of Gas Flow Dynamics in Transmission System

The gas flow dynamics can be utilized to expand the feasible region of IES operation. For example, as shown in Fig. 4, an EH is supplied by a gas source through a pipeline. During normal operation, the gas flows steadily, and the gas flow into the pipeline is equal to the gas flow out of the pipeline, i.e., $q_i = q_j$. When the

gas source fails, assume the gas production capacity is reduced to q'_i ($q'_i < q_i$). If we regulate this IES using the steady state gas flow model, the gas that flows out of the pipeline must be equal to the gas that flows into the pipeline, i.e., $q'_j = q'_i$. Then, the maximum available gas consumption of the EH is also reduced, i.e., $g_{13} + g_{14} \leq q'_j$. However, if we regulate the IES using the dynamic gas flow model, then the q'_j does not necessarily equal to q'_i . Instead, the maximum available gas consumption is a time-varying value $q''_j(t)$, which is governed by the dynamic gas flow equations ($q'_j \leq q''_j(t) \leq q_j$). Then, the gas consumption of the EH is subject to $g_{13} + g_{14} \leq q''_j(t)$. Therefore, the feasible region of the EH operation can be expanded with the dynamic gas flow model.

Gas flow dynamics can be described by continuity and motion equations [29]. The motion equation is nonlinear, which will cause the following optimal control problem intractable. To avoid this issue, here we can linearize the motion equations around the operating point by using the Taylor expansion technique

$$\partial_x \Delta p + 4\rho_0^2 B^2 q^* (F^2 D A^2 p^*)^{-1} \Delta q = 0 \quad (5)$$

where p and q are the gas pressure and gas flow along the pipeline with respect to time t and length x , respectively; p^* and q^* are the reference points of the gas pressure and gas flow functions in the Taylor expansion, respectively; The selections of the reference points are elaborated in Section V-A using a forward-approximation-based linearization technique. $\Delta p = p(x, t) - p(x, 0)$ and $\Delta q = q(x, t) - q(x, 0)$ are the increment of p and q around the operating point, respectively.

Using the finite difference scheme, the continuity and motion equations can be reformulated as

$$\frac{4\rho_0^2 B^2 q_m^*}{F^2 D A^2 p_m^*} \left(\frac{q_{m+1,k+1} + q_{m,k+1} + q_{m+1,k} + q_{m,k}}{4} - \frac{q_{m+1,0} + q_{m,0}}{2} \right) - \frac{p_{m+1,k+1} - p_{m,k+1} + p_{m+1,k} - p_{m,k}}{2\Delta x} - \frac{p_{m+1,0} - p_{m,0}}{\Delta x} = 0 \quad (6)$$

$$\Delta x A (p_{m+1,k+1} + p_{m,k+1} - p_{m+1,k} - p_{m,k}) + \Delta t \rho_0 B^2 (q_{m+1,k+1} - q_{m,k+1} + q_{m+1,k} - q_{m,k}) = 0 \quad (7)$$

where k is the index for discretized time step; Δx is the length of the pipeline segment; p_m^* and q_m^* is the reference points of the gas pressure and gas flow on the segment m , respectively; Δt is the time step. B is the isothermal wave speed of gas; ρ_0 is the density of gas at the standard temperature and pressure; A is the cross-sectional area of the pipeline; D is the diameter of the pipeline; F is the Fanning transmission factor.

After formulating the dynamic equations for all the pipelines, the initial conditions can be given by

$$p_{ij}|_{t=0} = \left((p_i^{(0)})^2 - \text{sgn}(p_i^{(0)} - p_j^{(0)}) (q_{ij}^{(0)})^2 (C_{ij}^2 L_{ij})^{-1} x \right)^{1/2} \quad (8)$$

$$q_{ij}|_{t=0} = q_{ij}^{(0)} \quad (9)$$

$$C_{ij}(p_i^2 - p_j^2) = q_{ij} |q_{ij}| \quad (10)$$

where the initial condition for gas pressure (8) is derived from the Weymouth (10); L_{ij} is the length of the pipeline ij ; $p_i^{(0)}$ and $q_{ij}^{(0)}$ are the gas pressure at GB i and gas flow in the pipeline ij , respectively, which can be solved in the steady-state based integrated electricity-gas optimal power flow (SIOPF) problem [30]; $\text{sgn}(x)$ is the signum function, where $\text{sgn}(x) = 1$ if $x \geq 0$, and $\text{sgn}(x) = -1$ if $x < 0$; C_{ij} is the characteristic parameter of the pipeline ij in the Weymouth (10).

Boundary conditions of the pipelines can be expressed as

$$\begin{cases} p_{ij}|_{x=0} = p_{i,j_1}|_{x=0} & (\forall j_1 \in \Omega_i^g) \\ p_{ij}|_{x=0} = p_{j_2,i}|_{x=L_{ij}} & (\forall j_2 \in \Omega_i^g) \end{cases} \quad (11)$$

$$\begin{aligned} w_i - g d_i - \sum_{j \in G_i^{gfu}} g_{i,j}^{gfu} / \xi_{i,j} - \sum_{e \in E_i} g_{i_e} \\ + \sum_{j \in \Omega_i^g} q_{ji}|_{x=L_{ji}} - \sum_{j \in \Omega_i^g} q_{ij}|_{x=0} = 0 \end{aligned} \quad (12)$$

where Ω_i^g is the set of GBs connected to GB i through gas pipelines; w_i is the gas production of the gas source at GB i ; $g d_i$ is the gas load; G_i^{gfu} is the set of gas-fired units at GB i ; $g_{i,j}^{gfu}$ is the electricity generation of the gas-fired unit j at GB i ; $\xi_{i,j}$ is the efficiency of the gas-fired unit; e is the index for EH; E_i is the set of EHs at GB i ; g_{i_e} is the gas consumption of the end-user e .

IV. LOOK-AHEAD CONTINGENCY MANAGEMENT SCHEME

When random failures of gas sources or generators occur, the IES could be transferred from the normal operating state to a contingency state [31]. For maintaining the IES reliability, on the supply side, the gas production from gas sources and the electricity generation from generators may be re-dispatched. On the demand side, the end-users can adjust the electricity and gas consumptions and the operating conditions of their devices. However, the end-users' demand may still be curtailed in some severe contingency states, and the reliability of the IES may be affected.

For enhancing the IES reliability, a look-ahead coordinated contingency management scheme (LaCMS) is proposed to fully utilize the flexibilities of end-users and gas flow dynamics, as illustrated in Fig. 5. In the normal operating state, the SIOPF is performed to determine the operating condition of the IES. When component failure happens, this normal operating condition sets the initial condition for the LaCMS. The LaCMS is implemented for a prespecified look-ahead horizon KD to obtain the optimal load curtailment and time-varying system conditions. It is implemented sequentially until the contingency state is over. It is worth noting that the selection of the look-ahead horizon KD is flexible [32]. It can be from hours to days, depending on the application scenarios of the reliability evaluation. It also depends on the frequencies of the state transition of the system, to better balance the computation efficiency and the accuracy.

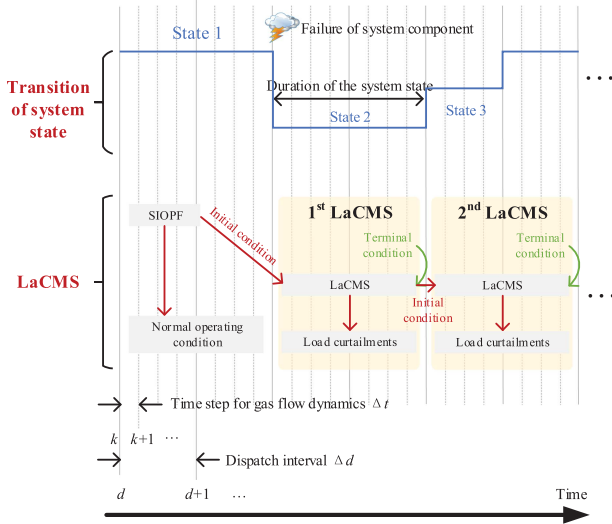


Fig. 5. Look-ahead contingency management scheme of the IES.

A. Operational Reliability Model of Components

To simulate the stochastic and chronological characteristics of the system state, the operational reliabilities of components are modeled using the discretized time Markov process. For a specific component, suppose the state at the current dispatch interval d is given. Then, the probabilities of the IES state in the next dispatch interval $d + 1$ can be calculated according to the following two scenarios.

- 1) The probability of IES remaining in its current state during the dispatch interval $d + 1$ can be calculated as

$$\Pr_0 = \prod_{r=1}^{NR} \frac{\Pr_r^{h_r}((d+1-d_r)\Delta d)}{\Pr_r^{h_r}(d-d_r)\Delta d} \quad (13)$$

where r is the index of the component; h_r is the state of the corresponding component in period d ; NR is the total number of components; d_r is the index of the beginning time period that component r is in the state h_r ; $\Pr_r^{h_r}(t)$ is the time-varying probability of component r in state h_r . The detailed calculation procedures are elaborated in Appendix. B.

- 2) The probability of component r transferring from the state h_r to h'_r can be calculated as

$$\Pr_r^{h_r, h'_r} = \prod_{r'=1}^{NR, r' \neq r} \frac{\Pr_{r'}^{h_{r'}}((d+1-d_{r'})\Delta d)}{\Pr_{r'}^{h_{r'}}(d-d_{r'})\Delta d} \times \frac{\Pr_r^{h'_r}((d+1-d_r)\Delta d)}{\Pr_r^{h_r}(d-d_r)\Delta d}. \quad (14)$$

The process abovementioned determines the system state in dispatch interval $d + 1$ according to the state in d . Repeat this process, we can obtain the chronological state sequence during the operation.

B. Look-Ahead Contingency Management Scheme of Integrated Energy Systems

Compared to the electricity system, the operating state of the gas system are continuous due to the dynamics of gas flow. Therefore, the optimal control framework is introduced to optimize the operating strategy of the IES over a given period. However, the system operator cannot be fully aware of the possible system state evolution in the following dispatch intervals. It only knows the current state and predicts the possible states in the next several dispatch intervals.

The objective of the LaCMS is to minimize the total operating cost over a certain time period. ‘‘Look-ahead’’ means that the optimal control decisions made at the current dispatch interval should impose certain limitations on the terminal condition to withstand future risks. Regarding this specific problem, it indicates that a reasonable linepack level should be maintained at the end of the current dispatch interval. The control variables of the LaCMS are from the IEGTS and end-users, respectively:

The control variables of the IEGTS at each time step k include: 1) the gas pressure $p_{m,k}$ and gas flow $q_{m,k}$ of the pipeline segment m ; 2) the gas production $w_{i,k}$ of the gas source at GB i ; 3) the electricity load curtailment $ec_{i,k}$ and gas load curtailments $gc_{i,k}$ at bus i ; 4) the electricity generation of the gas-fired unit $g_{i,j,k}^{gfu}$ and the electricity generation of traditional fossil unit $g_{i,j,k}^{tfu}$ at EB i ; 5) the voltage phase angle $\theta_{i,k}$ at EB i . The control variables of the end-user e at time step k include: 1) the electricity and gas consumption $ei_{e,k}$ and $gi_{e,k}$; 2) the electricity, heating, and cooling load curtailments $lc_{e,l}^l, l \in \{el, cl, ht\}$; 3) other state variables of the devices in the EH, as described in Section III-A. The objective function of LaCMS is

$$\text{Min } C^T = C^{\text{IEGS}} + \sum_{i \in I^E \cup I^G} \sum_{e \in E_i} C_e^{\text{EH}} \quad (15)$$

$$C^{\text{IEGS}} = \sum_{k \in KD} \left(\sum_{i \in I^E} \left(\sum_{j \in G_i^{tfu}} cst_{i,j}(g_{i,j,k}^{tfu}) + \text{CDF}^E ec_{i,k} \right) + \sum_{i \in I^G} \left(gp_{i,k} w_{i,k} + \text{CDF}^G gc_{i,k} \right) \right) \quad (16)$$

$$C_e^{\text{EH}} = \sum_{k \in KD} \sum_{l \in \{el, hl, cl\}} lc_{e,k}^l \text{CDF}^l \quad (17)$$

where (15) presents the total cost C^T , including the IEGTS operating cost C^{IEGS} and EH operating cost C_e^{EH} ; I^E and I^G are the sets of electricity and gas buses, respectively; (16) is the IEGTS operating cost, where KD is the set of time steps involved in this LaCMS. The first term in (16) is the electricity generation cost of traditional fossil units; G_i^{tfu} is the set of traditional fossil units at EB i ; $g_{i,j,k}^{tfu}$ is the generation of the traditional fossil unit; $cst_{i,j}$ is the cost function of traditional fossil unit j at EB i ; The second term is the electricity load curtailment cost; CDF^E is the customer damage functions (CDF) of electricity [33]; Third term is gas production cost; $gp_{i,k}$ is the gas purchasing price of the gas source at GB i ; Fourth term is the gas load curtailment

cost, where CDF^G is the CDF of gas; (17) represent the EH operating cost, which is the sum of EH load curtailment cost for all energy types $l \in \{el, hl, cl\}$ in all time period $k \in KD$.

The optimal control problem is subject to the following constraints at each time step k .

- 1) The electricity power flow constraints

$$\sum_{j \in G_i^{gfu}} g_{i,j,k}^{gfu} + \sum_{j \in G_i^{tfu}} g_{i,j,k}^{tfu} - ed_i - \sum_{e \in E_i} ei_{e,k} - \sum_{j \in \Omega_i^e} f_{ij,k} = 0 \quad (18)$$

$$f_{ij,k} = (\theta_{i,k} - \theta_{j,k}) / X_{ij} \quad (19)$$

$$|f_{ij,k}| \leq f_{ij}^+ \quad (20)$$

where (18) is the nodal balance for electricity; ed_i is the electricity load; $ei_{e,k}$ is the electricity consumption of EH at time step k ; $f_{ij,k}$ is the electricity power flow at branch ij ; (19) is the dc power flow equation; $\theta_{i,k}$ and X_{ij} are the phase angle of the voltage and the reactance of the branch, respectively; (20) is the power limit for the electricity branch, where f_{ij}^+ is the capacity of the branch ij .

- 2) The equation of gas flow dynamics and the boundary conditions in (6)–(12).
- 3) The upper and lower limits of components

$$g_{i,j}^{tfu-} \leq g_{i,j,k}^{tfu} \leq g_{i,j}^{tfu,h,+} \quad (21)$$

$$g_{i,j}^{gfu-} \leq g_{i,j,k}^{gfu} \leq g_{i,j}^{gfu,h,+} \quad (22)$$

$$w_i^- \leq w_{i,k} \leq w_i^{h,+} \quad (23)$$

where (21) is the electricity generation constraints for traditional fossil units; $g_{i,j}^{tfu-}$ and $g_{i,j}^{tfu,h,+}$ are the lower and upper bounds for the electricity generation of the gas-fired unit at state h , respectively; (22) is the electricity generation constraints for the gas-fired unit, where $g_{i,j}^{gfu-}$ and $g_{i,j}^{gfu,h,+}$ are the lower and upper bounds of the gas-fired unit at state h , respectively; (23) is the gas production constraints for the gas source; w_i^- and $w_i^{h,+}$ are the lower and upper bounds for the gas production of the gas source at state h . Note the electricity generation and gas production capacities of the components are determined by their random failures and repairs, as described in Section IV-A.

- 4) *Terminal conditions*: Terminal condition is set to avoid the abuse of linepack. Linepack is the gas stored in the pipeline, which is directly related to the nodal gas pressures. Keeping a sufficient linepack at the end of LaCMS is beneficial for the gas network to defend against future risks

$$p_{i,j,m,NK} \geq (1 - \omega)p_{i,j,m,1} \quad (24)$$

where $p_{i,j,m,1}$ represents the gas pressure at pipeline segment m in gas pipeline ij at time step $k = 1$; NK is the number of time steps involved in this LaCMS; ω

is the tolerance of the gas pressure fluctuation during the LaCMS.

It is also worth noting that ω is not always fixed. By setting different values of ω , the system operator can have tradeoffs between the reliability at the current moment and the reliability in the future. If the failures are too severe at the current moment, the system operator can set a higher ω to focus on solving the crisis at the current moment. By this means, the system operator can regulate the reliability more flexibly.

- 5) The operating constraints of end-users in (1)–(4).

V. OPERATIONAL RELIABILITY EVALUATION

A. Linearization of Gas Flow Dynamic Equations With a Forward-Approximation-Based Technique

In optimization-orientated researches, the reference point (6) can be selected as prespecified values, without causing too much inaccuracy [13]. This is because, in these researches, the change of system state is usually caused by the fluctuations of load and wind the impacts of which are relatively limited. However, in the reliability evaluation problem, due to component failures, the operating condition of the IES may change dramatically. Directly adopting the prespecified values as the reference point may cause unneglectable inaccuracies. Therefore, an adaptive linearization technique is devised in this article based on a forward-approximation method. The procedures to determine the reference point of a segment m in pipeline ij are as follows.

Step 1: Obtain the operating point of gas pressure and gas flow in the pipeline segment $p_{i,j,m}^{(0)}$ and $q_{i,j,m}^{(0)}$, by solving the optimal control problem in Section IV-B with all components being in the perfect function state.

Step 2: In each system state s , tentatively set $p_{i,j,m}^* = p_{i,j,m}^{(0)}$ and $q_{i,j,m}^* = q_{i,j,m}^{(0)}$. Solve the new optimal control problem with the reference points. Obtain the solutions of gas pressure and gas flow in each system state s as $p_{i,j,m,s}^{(1)}$ and $q_{i,j,m,s}^{(1)}$.

Step 3: The reference point of gas pressure can be obtained as follows [34] (the derivation process is elaborated in Appendix C). The reference point of gas flow can be calculated similarly

$$p_{i,j,m,s}^* = \frac{2}{3} \left(p_{i,j,m,s}^{(0)} + p_{i,j,m,s}^{(1)} - \frac{p_{i,j,m,s}^{(0)} p_{i,j,m,s}^{(1)}}{p_{i,j,m,s}^{(0)} + p_{i,j,m,s}^{(1)}} \right). \quad (25)$$

B. Operational Reliability Evaluation Procedures

Expected demand not supplied (EDNS), loss of load probability (LOLP), and expected energy not supplied (EENS) are widely adopted for the reliability evaluation of the electricity system [35]. On this basis, we design the indices for IES from two aspects. First, for evaluating the reliability of multiple energies, the indices of the electricity system are reformulated to expected gas not supplied (EGNS), loss of gas probability (LOGP), and

expected gas volume not supplied (EVNS), respectively. Moreover, for evaluating the time-varying reliability in the operational phase, the indices are further reformulated into time-varying values. The operational reliability of the gas system can be evaluated as

$$EGNS_i(k) = \left(\sum_{v=1}^{NV} gc_{i,k,v} \right) / NS \quad (26)$$

$$LOGP_i(k) = \left(\sum_{v=1}^{NV} \text{flag}(gc_{i,k,v}) \right) / NS \quad (27)$$

$$EVNS_i = \left(\sum_{v=1}^{NV} \sum_{k \in K} gc_{i,k,v} \right) / NS \quad (28)$$

where v is the index for the sampling time of the time-sequential Monte Carlo simulation; NV is the number of sampling times; $\text{flag}(x) = 1$ when $x > 0$, and $\text{flag}(x) = 0$ when $x \leq 0$.

The criterion for convergence can be evaluated by the relative standard deviation

$$\sqrt{\text{Var} \left(\sum_{k \in K} EDNS_i \right) / \sum_{k \in K} EDNS_i} \leq \xi \quad (29)$$

where $\text{Var}(x)$ is the variance of x ; K is the set of time steps in the operational horizon.

The operational reliability evaluation procedures are summarized as follows.

Step 1: Set the length of the studied operational period and the dispatch interval. Set the time step and length of the pipeline segment for the finite difference scheme. Set the state transition rate of the components.

Step 2: Generate the system state sequence in each dispatch interval according to (13), (14), including the gas production and electricity generation capacities of the gas sources, gas-fired units, and traditional fossil units, respectively.

Step 3: In each Monte Carlo simulation, observe whether the contingency state occurs. If it occurs, perform the SIOPF to determine the operating condition of the IES in the normal state. Set the solution of the operating condition as the initial condition for the optimal control problem. Otherwise, it indicates that the demands are not curtailed in this Monte Carlo simulation. Go to Step 6.

Step 4: Based on the state of the system component, update the electricity generation and gas production capacities of the corresponding components according to (21)–(23).

Step 5: Obtain the reference points of the linearization according to Section V-A. Solve the LaCMS model in Section IV-B to obtain the operating condition of the IES, as well as the electricity and gas load curtailments in each time step of the dispatchable interval.

Step 6: Repeat Step 4 and Step 5 until the operational period ends. Then, the electricity and gas load curtailments over the whole operational period can be obtained.

Step 7: Calculate the operational reliability indices according to (26)–(28). If (29) is satisfied, output the reliability indices as the final results. Otherwise, go to Step 1 and begin the next Monte Carlo simulation.

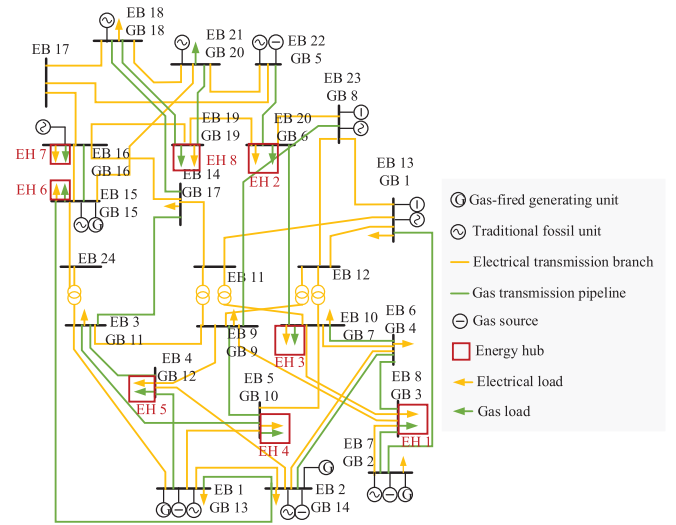


Fig. 6. Test system of the integrated energy system.

Since the number of length and time steps will affect the number of optimization variables, it is important to select proper step sizes Δx and Δt to improve the computation efficiency. The selection of Δt mainly considers two factors: The dispatch interval of the electricity system and the time constant of gas flow dynamics. Δt should not be longer than the dispatch interval of the power system. Otherwise, the electricity system cannot be dispatched based on the state change of the gas system. It should also reflect the middle state in the transient process of gas flow, which can improve the accuracy in determining the electricity generation of the gas-fired units and gas consumption of EHs. The selection of Δx is mainly subject to computation efficiency. It is widely demonstrated that the impact of larger Δx on the accuracy is limited. Thus, we can select a relatively large Δx to both improve the computation efficiency, and avoid numerical issues.

VI. CASE STUDIES

The proposed operational reliability evaluation technique is validated using an IES integrated by the IEEE Reliability Test System [36], the Belgium gas transmission systems [30], and the EH-based end-users [8], as presented in Fig. 6. The test system has 3405 MW electricity generation capacity and 48.966 Mm³/day gas production capacity in total. The electricity and gas loads of the IEGTS are 2850 MW and 46.298 Mm³/day, respectively. Compared with the original IEEE Reliability Test System, five 12 MW generators at EB 15, two 20 MW generators at EB 1, two 20 MW generators at EB 2, and three 100 MW generators at EB 7 are replaced by gas-fired units with the same generating capacities. Eight EHs are integrated at EB 8, 20, 10, 5, 4, 15, 16, and 19, respectively. Both the time step of gas flow dynamics and the dispatch interval are set as 15 min. Simulations are performed on a server with an E5-2678 2.50 GHz CPU and 64 GB RAM, using parallel computing techniques. The optimization model is solved using Gurobi commercial solver.

TABLE I
REPRESENTATIVE SYSTEM CONTINGENCY STATE SEQUENCE

| No. | Start | End | Description of the state |
|-----|-------|-------|--|
| S1 | 0:00 | 2:00 | Normal operation |
| S2 | 2:00 | 4:00 | Deration of the gas source at GB 1 by 2.32 Mm ³ /day |
| S3 | 4:00 | 6:00 | Deration of the gas source at GB 1 by 9.28 Mm ³ /day |
| S4 | 6:00 | 8:00 | Normal operation |
| S5 | 8:00 | 10:00 | Failures of a 400 MW generator at EB 18 (Gen #23) and a 155 MW generator at EB 23 (Gen #32) |
| S6 | 10:00 | 12:00 | Deration of the gas source at GB 1 by 9.28 Mm ³ /day. Failures of a 400 MW generator at EB 18 (Gen #23) and a 155 MW generator at EB 23 (Gen #32) |

TABLE II
COMPARISONS OF DIFFERENT METHODS

| Method | Computation time (s) | Mean relative error at GB 7 | Max relative error at GB 7 |
|--------|----------------------|-----------------------------|----------------------------|
| M1 | 0.98 | 0.40% | 3.26% |
| M2 | 102.44 | / | / |
| M3 | 1.45 | 2.84% | 11.01% |
| M4 | 0.50 | 2.90% | 11.61% |
| M5 | 1694.71 | 0.29% | 1.84% |
| M6 | 1.01 | 1.76% | 5.21% |

A. Case 1: Impacts of Flexibilities From End-Users and Gas Flow Dynamics on the IES Operation

Case 1 is a representative scenario for analyzing the impacts of flexibilities from end-users and gas flow dynamics on the IES operation. As presented in Table I, there are six system states S1-S6 from 0:00 to 12:00. The gas pressure is limited to within $\pm 20\%$ of the value in the normal operating state. The terminal condition for the gas pressure is set to 95% of the value in the normal operating state.

First, the proposed method is validated. Six state-of-art methods M1-M6 are compared. M1 is our proposed method. In M2, the full dynamics of the gas flow model are retained, and the model is nonlinear. It is solved by a general nonlinear solver (IPOPT). In M3, the second-order cone reformulation technique is used with tightening procedures [37]. In M4, the traditional linearization technique with a stationary reference point is used [38]. In M5, branching and cutting plane methods are used (which are used in the Gurobi for handling bilinear terms [39]). In M6, the McCormick envelope method is used [40]. The computation efficiencies of the six methods are presented in Table II.

As we can see, our method has a better balance between computation time and accuracy. The computation performance of M2 is set as the baseline. Because the full dynamics with nonlinearities are retained in M2, the computation time is relatively longer. Compared with M2, our method M1 significantly improves the computation efficiency by 99.04%, while the relative error is controlled within an acceptable range. Moreover, because our method is formulated based on linear optimization, it is more robust than nonlinear solvers. Because optimization usually gets very stressful during the reliability evaluation, such improvements in computation efficiency and robustness are essential. The performance is M3 is worse than M1 in terms of both computation efficiency and accuracy. Because the second-order-cone relaxation must be combined with tightening procedures, it is sensitive to the selection of penalty factors

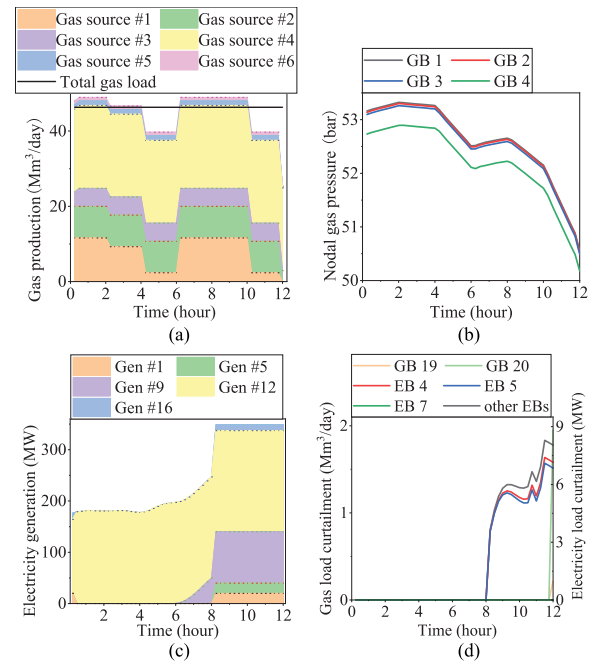


Fig. 7. Representative scenarios. (a) Gas production and total gas load. (b) Nodal gas pressure. (c) Electricity generation of representative generators. (d) Electricity and gas load curtailments.

during the tightening. Otherwise, it is easy to be stuck in the local optimum or nonoptimum value for the original problem. M4 is faster than M1, but the accuracies not satisfying either. M5 has the best accuracy, but the computation time is longer, which even becomes longer than M2. This is unacceptable, especially in reliability evaluations where the optimization problem will be solved numerous times. M6's performance is still a little worse than M1's. With better approximations of lower and upper bounds of optimization variables involved in McCormick envelopes, its performance is better than M3 and M6.

The optimization results of the IES by using the LaCMS are shown in Fig. 7. In Fig. 7(a), the total gas production from gas sources in S1 reaches their upper limits, which even exceeds the total gas load of the system. Thus, the linepack storage in the system is increased in S1. Meanwhile, as indicated in Fig. 7(b), the gas pressures at GBs 1, 2, 3, and 4 increase in S1 to prepare for possible gas supply shortages. In S2, the gas production from gas source #1 decreases due to its partial failure. The total gas production is lower than the total gas load, which causes a gradual decrease in gas pressure. In S3, though the gas production of gas source #1 drops dramatically, the gas load is not curtailed by using the proposed LaCMS, as shown in Fig. 7(d). Meanwhile, the nodal gas pressure only decreases slightly (e.g., the gas pressure at GB 1 decreases from 53.27 bar to 52.51 bar by 1.4%). When the system recovers the normal operation state S4, the total gas production exceeds the total gas load again. The linepack recovers.

Apart from adjusting the IEGTS, the end-users also reschedule their operating conditions, as presented in Fig. 8. For example, when a system failure occurs in S5, the end-user changes the operating point of CHP to replace electricity needs with gas. The electricity consumption of the end-user drops dramatically

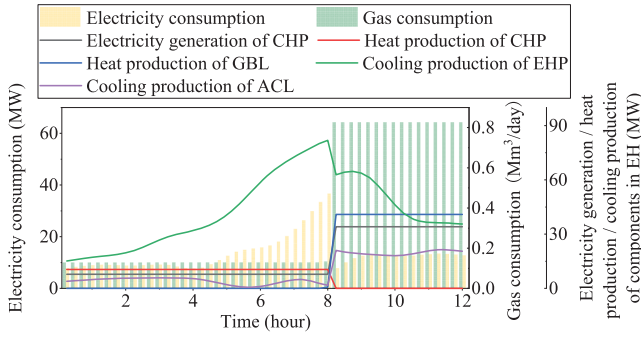


Fig. 8. Operating condition of the end-user.

by 78%, while the gas consumption increases by 511%. In the meantime, the nodal gas pressure also drops by 0.96%. Nonetheless, the electricity loads are still curtailed because the electricity system requires a real-time balance between the supply and demand sides, as presented in Fig. 7(d). In contrast, the gas load is not curtailed due to the gas flow dynamics. With the further failure of the gas source in S6, the nodal gas pressure approaches its lower limit, as shown in Fig. 7(b). The linepack also becomes insufficient. Thus, the gas loads are curtailed at the final moment 11:45-12:00, as shown in Fig. 7(d).

B. Case 2: Evaluation of IES Operational Reliabilities

Case 2 evaluates the IES operational reliabilities to reflect the joint impacts of gas flow dynamics and demand side flexibilities. Monte Carlo simulations are performed 1.5×10^5 times, and the reliability indices converge. The computation time is 5.45 h with the proposed method, which is acceptable for day-ahead evaluations.

First, scenarios A, B, and C are established to evaluate the impacts of different CDF values. The CDFs of gas are set to 1, 10, and 0.1 times of their original value in scenarios A, B, and C, respectively. The operational reliabilities of the end-users are presented in Fig. 9. As we can see, the operational reliabilities of both electricity and gas systems are near zero during 0:00-4:00 due to the low electricity and gas demands. Afterward, the four reliability indices increase to different degrees. For the electricity system, the EDNS and LOLP in scenario B are the highest, which means the electricity loads are more likely to be curtailed. On the contrary, for the gas system, the EGNS and LOGP in scenario B are the lowest, which means the gas loads are less likely to be curtailed. This illustrates the tradeoff of operational reliabilities between the electricity and gas systems. Although the EDNS in scenario C is much lower than in scenario A, the EGNS in scenario C is close to scenario A. This indicates that the gas load curtailment is more likely to be avoided due to the utilization of the linepack.

From the spatial dimension, the nodal reliabilities of the IES are presented in Table III. Comparing the nodal reliabilities in a single scenario, we can find that due to the large transmission capacity of the electricity branches, the nodal reliabilities in the electricity system are almost evenly distributed. On the contrary, the gas system presents a different pattern. GB 20 is located at

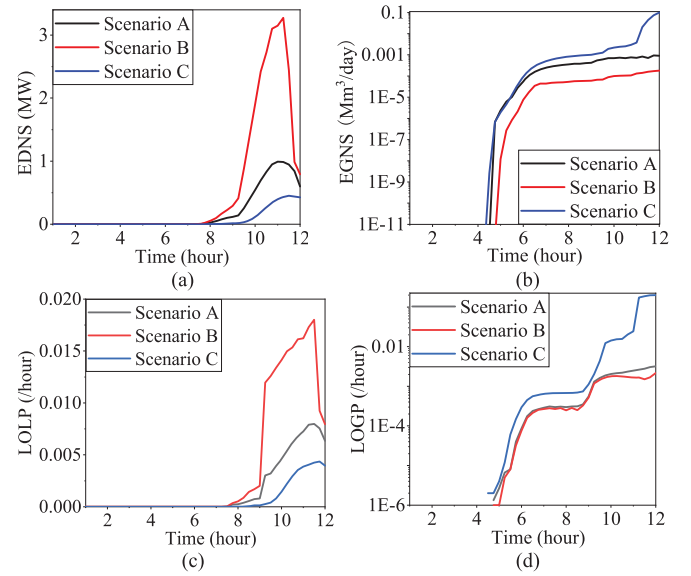


Fig. 9. Comparison with different customer damage functions. (a) EDNS. (b) EGNS. (c) LOLP. (d) LOGP.

TABLE III
NODAL EENS AND EGNS WITH DIFFERENT CDFs

| EENS (MWh) | | | |
|---------------------------------|-----------------------|-----------------------|-----------------------|
| Bus index | Scenario A | Scenario B | Scenario C |
| EB 7 | 0.1251 | 0.3515 | 0.0469 |
| Other EBs with electricity load | 0.1259 | 0.3527 | 0.0473 |
| EVNS (Mm ³) | | | |
| GB 3 | 6.66×10^{-6} | 4.35×10^{-6} | 1.55×10^{-5} |
| GB 6 | 7.81×10^{-6} | 7.18×10^{-6} | 1.47×10^{-5} |
| GB 7 | 6.08×10^{-6} | 4.37×10^{-6} | 1.39×10^{-5} |
| GB 10 | 5.25×10^{-6} | 1.47×10^{-6} | 1.37×10^{-5} |
| GB 12 | 5.16×10^{-6} | 1.91×10^{-6} | 1.40×10^{-5} |
| GB 15 | 6.76×10^{-6} | 4.59×10^{-6} | 1.55×10^{-5} |
| GB 16 | 1.09×10^{-5} | 6.71×10^{-6} | 2.80×10^{-5} |
| GB 19 | 8.46×10^{-6} | 2.96×10^{-6} | 2.29×10^{-5} |
| GB 20 | 7.35×10^{-5} | 2.33×10^{-5} | 2.40×10^{-3} |

the end of a pipeline route with no large gas source nearby. Its EVNS is significantly higher than other GBs. While other GBs near the gas source, such as GB 3, 6, and 7, have relatively higher reliabilities than other GBs. The distribution of nodal reliabilities in different scenarios presents a similar pattern as in Fig. 9. However, the different weights of electricity and gas CDFs have different impacts on different GBs. For example, the reliabilities of GB 20 are very different in scenarios A and C, which means increasing the gas CDF in this range can effectively improve the reliability. While in scenarios A and B, the impacts of the increase in the gas CDF are not that significant.

In summary, due to the different dynamics of electricity and gas, the ways of ensuring the reliabilities in the two systems are different. The electricity system usually ensures reliability by having redundant generation capacity. While in the gas system, the redundancy of gas production capacity is not high. Nonetheless, by utilizing the flexibility of linepack, its reliability can be also well guaranteed. However, it is worth noting that we should pay great attention to the redundancies of the transmission capacity of pipelines and nodal pressure limits. Otherwise, some

TABLE IV
EXPECTED OPERATING CONDITIONS OF IES WITH DIFFERENT TERMINAL CONDITIONS

| Scenario | D | E | F |
|---|-----------------------|-----------------------|--------------------|
| 0:00- EENS (MWh) | 0 | 0 | 0 |
| 6:00 Expected generation and load curtailment cost (\$) | 1.15×10^5 | 1.15×10^5 | 1.12×10^5 |
| Expected gas production (Mm^3) | 9.89 | 9.13 | 6.27 |
| Expected gas production cost (\$) | 7.02×10^5 | 6.37×10^5 | 3.94×10^5 |
| EVNS (Mm^3) | 0 | 0 | 0 |
| Expected gas load curtailment cost (\$) | 0 | 0 | 0 |
| Expected total operating cost (\$) | 8.17×10^5 | 7.52×10^5 | 5.06×10^5 |
| 6:00- EENS (MWh) | 0.95 | 1.06 | 462 |
| 12:00 Expected generation and load curtailment cost (\$) | 1.67×10^5 | 1.70×10^5 | 7.02×10^5 |
| Expected gas production (Mm^3) | 10.87 | 11.63 | 12.18 |
| Expected gas production cost (\$) | 7.85×10^5 | 8.50×10^5 | 8.96×10^5 |
| EVNS (Mm^3) | 2.07×10^{-7} | 1.32×10^{-5} | 0.1462 |
| Expected gas load curtailment cost (\$) | 2.25 | 142 | 1.58×10^6 |
| Expected total operating cost (\$) | 9.53×10^5 | 1.02×10^6 | 3.18×10^6 |

GBs may be vulnerable. Moreover, it is also validated that the different weights on the electricity and gas loads do lead to reliability tradeoffs between different energy systems.

Another three scenarios D, E, and F are constructed to evaluate the IES operational reliabilities with different terminal conditions. The operational horizon is divided into two time periods, 0:00–6:00 and 6:00–12:00, respectively. The terminal conditions of gas pressure at 6:00 are set to 1, 0.98, and 0.9 times of the normal values, respectively. At 12:00 the terminal conditions are all set to 0.95 times of the value in the normal operation. The limits for the gas pressure fluctuation are all set as $\pm 10\%$.

Table IV presents the reliability indices and the expected cost in scenarios D, E, and F. The total operating cost and operational reliability over the 12 h in scenario D are better than in scenarios E and F, because the terminal condition of gas pressure at 6:00 in scenario D is the highest. Although the reliability in 0:00–6:00 in scenario D is a little inferior, the reliability in 6:00–12:00 is improved significantly. This further indicates that maintaining sufficient linepack is vital to guarantee the operational reliability of the IES over the entire operational horizon.

C. Case 3: Long-Term Evaluation Results

In this case, we use a practical dataset to conduct a long-term evaluation, so as to demonstrate the effectiveness of the proposed method. The gas and electricity demands are normalized according to the practical electricity and gas demand curves in the U.K. from Feb. 16–23, 2023 [41], [42], as shown in Fig. 10. Four scenarios are set to validate the proposed LaCMS and reliability evaluation techniques. S1 is the base scenario. In S2, the weight of gas demand is promoted. In S3, the weight of electricity demand is promoted. In S4, the look-ahead horizon is set as a week, and the terminal condition of gas pressure is set according to the long-term prediction value of gas demand. When gas demand exceeds the average value of this week, the terminal condition of gas pressure is set to 0.98 times of its normal value. When the gas demand is lower than the average value, the terminal condition is set to 1.02 times of its normal value.

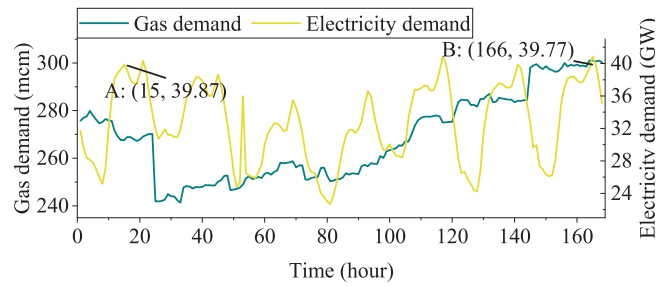


Fig. 10. Weekly electricity and gas demand curves in U.K. on Feb. 16–23, 2023.

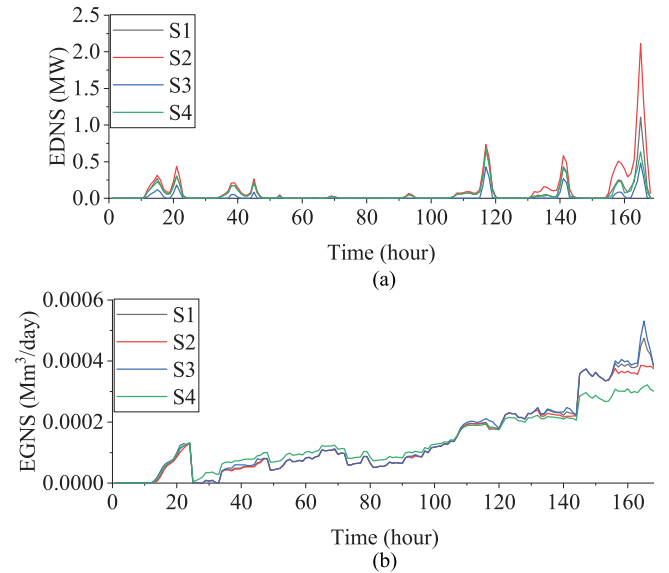


Fig. 11. Operational reliabilities of the IES in different scenarios. (a) EDNS. (b) EGNS.

The operational reliabilities of the IES in different scenarios are presented in Fig. 11.

First, we find that although the reliability indices follow the pattern of the demand curve (EDNS or EGNS is higher with higher electricity or gas demand), they generally grow over time. Even if the demand is almost the same (e.g., points A and B, as shown in Fig. 10), the reliability indices at a later time are higher than that at an earlier time. This is because we have observed that the IES components are normal at $t = 0$. As time grows, the failure probability of components will become higher.

Comparing S1, S2, and S3, we validate the reliability tradeoffs between different energy systems. For example, as the weight of the gas demand increases in S2, the EDNS in S2 is higher than that in S1. In contrast, the EGNS in S2 is lower than in S1. This effect is more obvious at the later period (e.g., $t = 155$ – 168 h) when the failure probabilities of IES components are higher.

Comparing S1 and S4, we validate the reliability tradeoffs between different time periods. For example, as shown in Fig. 11(b), before $t = 108$ h, the EGNS in S4 is higher than in S1. After that, the EGNS in S4 is lower than in S1. This is because the system operator regulates the linepack according to the long-term prediction of gas demand. When gas demand

is low, the terminal condition of gas pressure is high, which increases the linepack in the gas network. This linepack can be committed when the gas demand is high to improve reliability. For example, from 145–168 h, the EGNS decreases significantly by 22.64%. Moreover, over the entire operating horizon, the gas system reliability is improved by 3.91%. It validates that our method can help the system operator to flexibly manage the reliabilities among different time periods, so as to improve the overall reliabilities during the operation.

VII. CONCLUSION

With the coordination of the electricity, gas, and heat energies, the IES presents substantially different dynamics and flexibilities compared to the traditional electricity system. This article proposed an operational reliability evaluation technique for the IES considering flexibilities from both the gas flow dynamics in the transmission system and the end-users on the demand side. By developing a look-ahead contingency management scheme, we can manage and improve the operational reliability of IES in terms of both different energy systems and time periods.

From numerical studies, we first validate that the computation efficiency of our method is 99.04% higher than traditional methods. It also shows that by using flexibilities from the transmission system and demand side, the operational reliabilities in terms of different time periods and energy systems can be well balanced

and enhanced. For example, by properly setting the terminal conditions, the EVNS of the gas system can be improved by 0.15 Mm³/day. The total operating cost can also be improved by 51.98%. It is also validated using a practical dataset that our method can improve the operational reliability during the load peak hours by 22.64%.

With the ever-increasingly tight integration of multiple energies, the reliability issues caused by this coupling relationship bring our attention. However, we should also not neglect that this integration enables more flexibility in the IES, which can also be an opportunity in improving reliabilities. Against this background, the quantitative results and reliability evaluation framework in our study can bring new perspectives to the system operator in terms of reliability management. It can also be applied to the day-ahead or hourly schedule to ensure reliability in the IES.

APPENDIX

A. Specific Elements in the EH Model

The specific elements of the matrices in the EH model are elaborated as follows. In the EH model, as shown in Fig. 3, the energy flows (i.e., electricity, gas, heat, and cooling flows) between two nodes n_1 and n_2 are represented as e_{n_1, n_2} , g_{n_1, n_2} , h_{n_1, n_2} , and c_{n_1, n_2} , respectively. The set of state variables \mathbf{x} ,

$$\underbrace{\begin{bmatrix} \eta_3^e & 0 & 0 & 0 & -1 & -1 & 0 & 0 & 0 & 0 & 0 & 0 & 0 \\ \eta_3^g & 0 & 0 & 0 & 0 & 0 & -1 & -1 & 0 & 0 & 0 & 0 & 0 \\ 0 & \eta_4 & 0 & 0 & 0 & 0 & 0 & 0 & -1 & -1 & 0 & 0 & 0 \\ 0 & 0 & \gamma \text{COP}_5^h & 0 & 0 & 0 & 0 & 0 & 0 & 0 & -1 & 0 & 0 \\ 0 & 0 & (1-\gamma)\text{COP}_5^c & 0 & 0 & 0 & 0 & 0 & 0 & 0 & 0 & -1 & 0 \\ 0 & 0 & 0 & 0 & 0 & 0 & \text{COP}_6 & \text{COP}_6 & 0 & 0 & 0 & 0 & -1 \\ 0 & 0 & 0 & 1 & 0 & 1 & 0 & 0 & 0 & 0 & 0 & 0 & 0 \\ 0 & 0 & 0 & 0 & 0 & 0 & 0 & 1 & 0 & 1 & 1 & 0 & 0 \\ 0 & 0 & 0 & 0 & 0 & 0 & 0 & 0 & 0 & 0 & 0 & 1 & 1 \end{bmatrix}}_{\mathbf{H}} \underbrace{\begin{bmatrix} g_{13} \\ g_{14} \\ e_{25} \\ e_{27} \\ e_{35} \\ e_{37} \\ h_{36} \\ h_{38} \\ h_{46} \\ h_{48} \\ h_{58} \\ c_{59} \\ c_{69} \end{bmatrix}}_{\mathbf{x}} = \begin{bmatrix} 0 \\ 0 \\ 0 \\ 0 \\ 0 \\ 0 \\ 0 \\ d^{el} - lc^{el} \\ d^{hl} - lc^{hl} \\ d^{cl} - lc^{cl} \end{bmatrix} \quad (30)$$

$$\underbrace{\begin{bmatrix} 0 & 0 & 0 & 0 & 1 & 1 & -\frac{E_A-E_B}{H_A-H_B} & -\frac{E_A-E_B}{H_A-H_B} & 0 & 0 & 0 & 0 & 0 \\ 0 & 0 & 0 & 0 & -1 & -1 & \frac{E_B-E_C}{H_B-H_C} & \frac{E_B-E_C}{H_B-H_C} & 0 & 0 & 0 & 0 & 0 \\ 0 & 0 & 0 & 0 & -1 & -1 & \frac{H_B-H_C}{E_C-E_D} & \frac{H_B-H_C}{E_C-E_D} & 0 & 0 & 0 & 0 & 0 \\ 0 & 0 & 0 & 0 & 0 & 0 & 0 & 0 & -1 & -1 & 0 & 0 & 0 \\ 0 & 0 & 0 & 0 & 0 & 0 & 0 & 0 & 1 & 1 & 0 & 0 & 0 \\ 0 & 0 & 0 & 0 & 0 & 0 & 0 & 0 & 0 & 0 & -1 & 0 & 0 \\ 0 & 0 & 0 & 0 & 0 & 0 & 0 & 0 & 0 & 0 & 1 & 0 & 0 \\ 0 & 0 & 0 & 0 & 0 & 0 & 0 & 0 & 0 & 0 & 0 & -1 & 0 \\ 0 & 0 & 0 & 0 & 0 & 0 & 0 & 0 & 0 & 0 & 0 & 0 & -1 \\ 0 & 0 & 0 & 0 & 0 & 0 & 0 & 0 & 0 & 0 & 0 & 0 & 1 \end{bmatrix}}_{\mathbf{A}} \underbrace{\begin{bmatrix} g_{13} \\ g_{14} \\ e_{25} \\ e_{27} \\ e_{35} \\ e_{37} \\ h_{36} \\ h_{38} \\ h_{46} \\ h_{48} \\ h_{58} \\ c_{59} \\ c_{69} \end{bmatrix}}_{\mathbf{x}} + \underbrace{\begin{bmatrix} E_B - \frac{-E_A}{H_B(E_B-E_C)} \\ E_D \\ -ho_2^- \\ ho_2^+ \\ \gamma ho_3^- \\ \gamma ho_3^+ \\ -(1-\gamma)co_3^- \\ (1-\gamma)co_3^+ \\ -co_4^- \\ co_4^+ \end{bmatrix}}_{\mathbf{B}} \leq \mathbf{0}. \quad (31)$$

matrices \mathbf{A} and \mathbf{B} are vectors, which are shown in (30) and (31) shown at the bottom of this page. (E_A, H_A) , (E_B, H_B) , (H_C, E_C) , and (H_D, E_D) are four extreme points of the feasible region; COP_3^h and COP_3^c are the coefficients of performance of the EHP in heating and cooling mode, respectively; η_1^e and η_1^h are the electrical and thermal efficiencies of the CHP; η_2 is the thermal efficiency of the GBL; COP_4 is the coefficient of performance of the ACL; ho_2^+ and ho_2^- are the maximum and minimum heat capacities of GBL, respectively; ho_3^+ , co_3^+ and ho_3^- , co_3^- are the maximum and minimum heat and cooling capacities of EHP, respectively; co_4^+ and co_4^- are the maximum and minimum heat capacities of ACL, respectively; γ is the indicator for EHP operating mode, where $\gamma = 1$ represents heating mode, and $\gamma = 0$ represents cooling mode

B. Calculation Procedures of State Transition Probabilities

The time-varying state probability is used for characterizing the operational reliability of components and simulating system state transitions in Section IV-A. Generally, for a system component with NH states, the state transition process can be described by the Markov process [43]. The probability of the component $\text{Pr}^h(t)$ in the state h can be calculated by solving the following partial derivative equations:

$$\begin{cases} \frac{d\text{Pr}^h(t)}{dt} = -\text{Pr}^h(t) \sum_{h'=1}^{NH, h' \neq h} \lambda_{h, h'} \\ + \sum_{h'=1}^{NH, h' \neq h} \text{Pr}^{h'}(t) \lambda_{h', h} \\ h = 1, 2, \dots, NH \\ \text{Pr}^1|_{t=0} = 1, \text{Pr}^2|_{t=0} = \dots = \text{Pr}^{NH}|_{t=0} = 0 \end{cases} \quad (32)$$

where $\lambda_{h, h'}$ is the state transition rate from state h to h' .

Then, the probability of component r being in state h_r with respect to time can be represented as $\text{Pr}_r^{h_r}(t)$. Suppose the component r is transferred from state h_0 to state h_r at dispatch interval d_r . Under this condition, the probability of component r being in state h_r at dispatch interval d ($d > d_r$) can be represented by $\text{Pr}_r^{h_r}((d - d_r)\Delta d)$. Similarly, the probability of component r being in state h_r at dispatch interval $d + 1$ can be represented by $\text{Pr}_r^{h_r}((d + 1 - d_r)\Delta d)$. Then, the conditional probability of component r remains h_r at $d + 1$ can be derived as

$$\frac{\text{Pr}_r^{h_r}((d + 1 - d_r)\Delta d)}{\text{Pr}_r^{h_r}((d - d_r)\Delta d)} \quad (33)$$

Similarly, the conditional probability of component r transferred to state h'_r at $d + 1$ while it is at state h_r at d can be calculated by

$$\frac{\text{Pr}_r^{h'_r}((d + 1 - d'_r)\Delta d)}{\text{Pr}_r^{h_r}((d - d_r)\Delta d)} \quad (34)$$

Above is the calculation of state probability for a single component. Generally, for IES, it has NR components. Then, the conditional probability of only component r being transferred from h_r to h'_r at $d + 1$ (while other components remain in their

states h_r) can be obtained as

$$\begin{aligned} \frac{\text{Pr}_r^{h_r, h'_r}}{\text{Pr}_r^{h_r}} &= \left(\prod_{r'=1}^{NR, r' \neq r} \frac{\text{Pr}_{r'}^{h_{r'}}((d + 1 - d_{r'})\Delta d)}{\text{Pr}_{r'}^{h_{r'}}((d - d_{r'})\Delta d)} \right) \\ &\times \frac{\text{Pr}_r^{h'_r}((d + 1 - d'_r)\Delta d)}{\text{Pr}_r^{h_r}((d - d_r)\Delta d)}. \end{aligned} \quad (35)$$

C. Derivation Process of Reference Point

The reference point in (6) of a certain optimization variable (e.g., gas pressure or gas flow) is set according to the average value in the corresponding segment. Taking the gas pressure as an example, since it is governed by the Weymouth equation, we have (assuming we have a prespecified gas flow direction from bus i to j)

$$p_{ij, m}^2 - p_{ij, m+1}^2 = \Theta_{ij}^2 \Delta x_{ij} q_{ij, m}^2 \quad (36)$$

where Θ_{ij} is the property coefficient of pipeline ij . Then, the average pressure in the pipeline can be calculated as

$$\begin{aligned} p_{ij, m}^* &= \int_0^{\Delta x_{ij}} \sqrt{p_{ij, m}^2 - \Theta_{ij}^2 q_{ij, m}^2 x} dx \\ &= \frac{1}{\Theta_{ij}^2 q_{ij, m}^2} \int_{p_{ij, m+1}^2}^{p_{ij, m}^2} y^{\frac{1}{2}} dy \\ &= \frac{2}{3} \left(p_{ij, m} + p_{ij, m+1} - \frac{p_{ij, m} p_{ij, m+1}}{p_{ij, m} + p_{ij, m+1}} \right). \end{aligned} \quad (37)$$

Then, it can be set as the reference point of the motion equation.

REFERENCES

- [1] S. Wang, J. Zhai, and H. Hui, "Optimal energy flow in integrated electricity and gas systems with injection of alternative gas," *IEEE Trans. Sustain. Energy*, to be published, doi: 10.1109/TSTE.2023.3237229.
- [2] Y. Li, Z. Li, F. Wen, and M. Shahidehpour, "Privacy-preserving optimal dispatch for an integrated power distribution and natural gas system in networked energy hubs," *IEEE Trans. Sustain. Energy*, vol. 10, no. 4, pp. 2028–2038, Oct. 2019.
- [3] M. Alipour, K. Zare, and M. Abapour, "MINLP probabilistic scheduling model for demand response programs integrated energy hubs," *IEEE Trans. Ind. Inform.*, vol. 14, no. 1, pp. 79–88, Jan. 2018.
- [4] M. Geidl, G. Koeppel, P. Favre-Perrod, and B. Klockl, "Energy hubs for the future," *IEEE Power Energy Mag.*, vol. 5, no. 1, pp. 24–30, Jan./Feb. 2007.
- [5] G. Li, Z. Bie, Y. Kou, J. Jiang, and M. Bettinelli, "Reliability evaluation of integrated energy systems based on smart agent communication," *Appl. Energy*, vol. 167, pp. 397–406, Apr. 2016.
- [6] C. Yan, Z. Bie, S. Liu, D. Urgun, C. Singh, and L. Xie, "A reliability model for integrated energy system considering multi-energy correlation," *J. Modern Power Syst. Clean Energy*, vol. 9, no. 4, pp. 811–825, Feb. 2021.
- [7] W. Huang et al., "Reliability and vulnerability assessment of multi-energy systems: An energy hub based method," *IEEE Trans. Power Syst.*, vol. 36, no. 5, pp. 3948–3959, Sep. 2021.
- [8] S. Wang, H. Hui, Y. Ding, C. Ye, and M. Zheng, "Operational reliability evaluation of urban multi-energy systems with equivalent energy storage," *IEEE Trans. Ind. Appl.*, vol. 59, no. 2, pp. 1–15, Mar./Apr. 2023.
- [9] C. Juanwei, Y. Tao, X. Yue, C. Xiaohua, Y. Bo, and Z. Baomin, "Fast analytical method for reliability evaluation of electricity-gas integrated energy system considering dispatch strategies," *Appl. Energy*, vol. 242, pp. 260–272, May 2019.
- [10] Z. Zeng, T. Ding, Y. Xu, Y. Yang, and Z. Y. Dong, "Reliability evaluation for integrated power-gas systems with power-to-gas and gas storages," *IEEE Trans. Power Syst.*, vol. 35, no. 1, pp. 571–583, Jan. 2020.

- [11] Y. Tang, Y. Zhao, W. Li, K. Xie, and J. Yu, "Incorporating compressor station multiple failure modes in risk evaluation of electricity-gas integrated energy systems," *CSEE J. Power Energy Syst.*, to be published, doi: [10.17775/CSEEJPES.2020.05850](https://doi.org/10.17775/CSEEJPES.2020.05850).
- [12] Y. Zhou, C. Gu, H. Wu, and Y. Song, "An equivalent model of gas networks for dynamic analysis of gas-electricity systems," *IEEE Trans. Power Syst.*, vol. 32, no. 6, pp. 4255–4264, Nov. 2017.
- [13] Z. Bao, D. Chen, L. Wu, and X. Guo, "Optimal inter- and intra-hour scheduling of islanded integrated-energy system considering linepack of gas pipelines," *Energy*, vol. 171, pp. 326–340, Mar. 2019.
- [14] S. Clegg and P. Mancarella, "Integrated modeling and assessment of the operational impact of power-to-gas (P2G) on electrical and gas transmission networks," *IEEE Trans. Sustain. Energy*, vol. 6, no. 4, pp. 1234–1244, Oct. 2015.
- [15] L. Yan, X. Chen, Y. Chen, and J. Wen, "A cooperative charging control strategy for electric vehicles based on multiagent deep reinforcement learning," *IEEE Trans. Ind. Inform.*, vol. 18, no. 12, pp. 8765–8775, Dec. 2022.
- [16] H. Hui et al., "A transactive energy framework for inverter-based HVAC loads in a real-time local electricity market considering distributed energy resources," *IEEE Trans. Ind. Inform.*, vol. 18, no. 12, pp. 8409–8421, Dec. 2022.
- [17] P. Palensky and D. Dietrich, "Demand side management: Demand response, intelligent energy systems, and smart loads," *IEEE Trans. Ind. Inform.*, vol. 7, no. 3, pp. 381–388, Aug. 2011.
- [18] N. Zhao, B. Wang, L. Bai, and F. Li, "Quantitative model of the electricity-shifting curve in an energy hub based on aggregated utility curve of multi-energy demands," *IEEE Trans. Smart Grid*, vol. 12, no. 2, pp. 1329–1345, Mar. 2021.
- [19] M. Z. Oskouei, B. Mohammadi-Ivatloo, M. Abapour, M. Shafiee, and A. Anvari-Moghaddam, "Strategic operation of a virtual energy hub with the provision of advanced ancillary services in industrial parks," *IEEE Trans. Sustain. Energy*, vol. 12, no. 4, pp. 2062–2073, Oct. 2021.
- [20] J. Yang, N. Zhang, C. Kang, and Q. Xia, "Effect of natural gas flow dynamics in robust generation scheduling under wind uncertainty," *IEEE Trans. Power Syst.*, vol. 33, no. 2, pp. 2087–2097, Mar. 2018.
- [21] A. Zlotnik, L. Roald, S. Backhaus, M. Chertkov, and G. Andersson, "Coordinated scheduling for interdependent electric power and natural gas infrastructures," *IEEE Trans. Power Syst.*, vol. 32, no. 1, pp. 600–610, Jan. 2017.
- [22] G. Koeppel and G. Andersson, "Reliability modeling of multi-carrier energy systems," *Energy*, vol. 34, no. 3, pp. 235–244, Mar. 2009.
- [23] S. Wang, C. Shao, Y. Ding, and J. Yan, "Operational reliability of multi-energy customers considering service-based self-scheduling," *Appl. Energy*, vol. 254, Nov. 2019, Art. no. 113531.
- [24] W. Huang, Y. Wang, N. Zhang, C. Kang, W. Xi, and M. Huo, "Fast multi-energy systems reliability evaluation using multi-parametric linear programming," in *Proc. IEEE Power Energy Soc. Gen. Meeting*, 2019, pp. 1–5.
- [25] S. Wang, Y. Ding, X. Han, P. Wang, L. Goel, and J. Ma, "Short-term reliability evaluation of integrated electricity and gas systems considering dynamics of gas flow," *IET Gener., Transmiss. Distrib.*, vol. 15, no. 20, pp. 2857–2871, Jun. 2021.
- [26] M. Bao, Y. Ding, C. Shao, Y. Yang, and P. Wang, "Nodal reliability evaluation of interdependent gas and power systems considering cascading effects," *IEEE Trans. Smart Grid*, vol. 11, no. 5, pp. 4090–4104, Sep. 2020.
- [27] M. Cao et al., "Reliability assessment of integrated energy systems considering emergency dispatch based on dynamic optimal energy flow," *IEEE Trans. Sustain. Energy*, vol. 13, no. 1, pp. 290–301, Jan. 2022.
- [28] M. Bao, Y. Ding, X. Yin, C. Shao, and C. Ye, "Definitions and reliability evaluation of multi-state systems considering state transition process and its application for gas systems," *Rel. Eng. Syst. Saf.*, vol. 207, Mar. 2021, Art. no. 107387.
- [29] I. Cameron, "Using an excel-based model for steady-state and transient simulation," in *Proc. PSIG Annu. Meeting*, 1999, pp. 1–38.
- [30] S. Wang, Y. Ding, C. Ye, C. Wan, and Y. Mo, "Reliability evaluation of integrated electricity-gas system utilizing network equivalent and integrated optimal power flow techniques," *J. Modern Power Syst. Clean Energy*, vol. 7, no. 6, pp. 1523–1535, Oct. 2019.
- [31] Y. Chen et al., "Self-triggered coordination of distributed renewable generators for frequency restoration in islanded microgrids: A low communication and computation strategy," *Adv. Appl. Energy*, vol. 10, Jun. 2023, Art. no. 100128.
- [32] Y. Chen et al., "Distributed self-triggered control for frequency restoration and active power sharing in islanded microgrids," *IEEE Trans. Ind. Inform.*, to be published, doi: [10.1109/TII.2023.3240738](https://doi.org/10.1109/TII.2023.3240738).
- [33] G. Wacker and R. Billinton, "Customer cost of electric service interruptions," *Proc. IEEE*, vol. 77, no. 6, pp. 919–930, Jun. 1989.
- [34] N. Keyaerts, M. Hallack, J.-M. Glachant, and W. D'haeseleer, "Gas market distorting effects of imbalanced gas balancing rules: Inefficient regulation of pipeline flexibility," *Energy Policy*, vol. 39, no. 2, pp. 865–876, Feb. 2011.
- [35] R. Billington and R. N. Allan, *Reliability Evaluation of Power Systems*. New York, NY, USA: Plenum, 1984.
- [36] C. Grigg et al., "The IEEE reliability test system-1996. A report prepared by the reliability test system task force of the application of probability methods subcommittee," *IEEE Trans. Power Syst.*, vol. 14, no. 3, pp. 1010–1020, Aug. 1999.
- [37] S. Chen, Z. Wei, G. Sun, D. Wang, and H. Zang, "Steady state and transient simulation for electricity-gas integrated energy systems by using convex optimisation," *IET Gener., Transmiss. Distrib.*, vol. 12, no. 9, pp. 2199–2206, Mar. 2018.
- [38] C. Zheng, J. Fang, S. Wang, X. Ai, Z. Liu, and Z. Chen, "Energy flow optimization of integrated gas and power systems in continuous time and space," *IEEE Trans. Smart Grid*, vol. 12, no. 3, pp. 2611–2624, May 2020.
- [39] "Non-convex quadratic optimization with Gurobi." [Online]. Available: https://co-at-work.zib.de/slides/Montag_21.9/luce_slides.pdf
- [40] S. Mhanna, I. Saedi, and P. Mancarella, "Iterative LP-based methods for the multiperiod optimal electricity and gas flow problem," *IEEE Trans. Power Syst.*, vol. 37, no. 1, pp. 153–166, Jun. 2022.
- [41] "Gas Operational Data community." [Online]. Available: <https://datacommunity.nationalgridgas.com/>
- [42] "Energy dashboard." [Online]. Available: <https://www.energydashboard.co.uk/historical>
- [43] Y. Ding, C. Singh, L. Goel, J. Østergaard, and P. Wang, "Short-term and medium-term reliability evaluation for power systems with high penetration of wind power," *IEEE Trans. Sustain. Energy*, vol. 5, no. 3, pp. 896–906, Jul. 2014.



Sheng Wang (Member, IEEE) received the Ph.D. and B.Eng. degrees in electrical engineering from Zhejiang University, Hangzhou, China, in 2021 and 2016, respectively.

He is currently a Postdoctoral Fellow with the State Key Laboratory of Internet of Things for Smart City, University of Macau. His research interests include optimization and reliability evaluation of integrated energy systems, and the low-carbon strategy for urban energy systems.



Junyi Zhai (Member, IEEE) received the B.S. and Ph.D. degrees in electrical engineering from North China Electricity Power University, Beijing, China, in 2014 and 2019, respectively.

He was a visiting student with the University of Birmingham during 2018 and 2019. He was a Senior Research Engineer with the State Grid (Suzhou) City and Energy Research Institute during 2019 and 2021. His research interests include mathematical optimization techniques and power system analysis and computing.



Hongxun Hui (Member, IEEE) received the B.E. and Ph.D. degrees in electrical engineering from Zhejiang University, Hangzhou, China, in 2015 and 2020, respectively.

From 2018 to 2019, he was a visiting scholar with the Advanced Research Institute, Virginia Tech, and the CURENT Center, University of Tennessee. He is currently a Research Assistant Professor with the State Key Laboratory of Internet of Things for Smart City, University of Macau, Macao SAR, China. His research interests include optimization and control of power system, demand response, and Internet of Things technologies for smart energy.



Yi Ding (Member, IEEE) received the bachelor's degree from Shanghai Jiaotong University, Shanghai, China, in 2000, and the Ph.D. degree from Nanyang Technological University, Singapore in 2007, both in electrical engineering.

He is currently a Professor with the College of Electrical Engineering, Zhejiang University, Hangzhou, China. His research interests include power systems reliability and performance analysis incorporating renewable energy resources, and engineering systems reliability modeling and optimization.



Yonghua Song (Fellow, IEEE) received the B.E. degree from Chengdu University of Science and Technology, Chengdu, China, in 1984, and the Ph.D. degree from China Electric Power Research Institute, Beijing, China, in 1984, both in electrical engineering.

From 1989 to 1991, he was a Postdoctoral Fellow with Tsinghua University, Beijing, China. He then held various positions with Bristol University, Bristol, U.K.; Bath University, Bath, U.K.; John Moores University, Liverpool, U.K., from 1991 to 1996. In 1997, he was a Professor of Power Systems with Brunel University, where he has been a Pro-Vice Chancellor for Graduate Studies since 2004. In 2007, he took up a Pro-Vice Chancellorship and Professorship of Electrical Engineering with the University of Liverpool, Liverpool. In 2009, he was with Tsinghua University as a Professor of Electrical Engineering and an Assistant President and the Deputy Director with the Laboratory of Low-Carbon Energy. During 2012 to 2017, he was the Executive Vice President with Zhejiang University, as well as Founding Dean of the International Campus and Professor of Electrical Engineering and Higher Education of the University. Since 2018, he has been Rector of the University of Macau and the Director with the State Key Laboratory of Internet of Things for Smart City. His current research interests include smart grid, electricity economics, and operation and control of power systems.

Dr. Song was elected as the Vice-President of Chinese Society for Electrical Engineering (CSEE) and appointed as the Chairman of the International Affairs Committee of the CSEE in 2009. In 2004, he was elected as a Fellow of the Royal Academy of Engineering, U.K. In 2019, he was elected as a Foreign Member of the Academia Europaea. He was the recipient of D.Sc. by Brunel University in 2002, Honorary D.Eng. by the University of Bath in 2014, and Honorary D.Sc. by the University of Edinburgh in 2019.